Benchmark experiments for moisture transfer modelling in air and porous materials

In: Building and Environment, 46(4), pp. 884-898, 2011

Benchmark experiments for moisture transfer modelling in air and porous materials

M. Van Belleghem[1], M. Steeman[2], A. Willockx[1], A. Janssens[2] and M. De Paepe[1]

[1] Ghent University, Department of Flow, Heat and Combustion Mechanics, Sint-Pietersnieuwstraat 41, B-9000 Ghent, Belgium
[2] Ghent University, Department of Architecture and Urban Planning, Jozef Plateaustraat 22, B-9000 Ghent, Belgium

Corresponding author: Marnix Van Belleghem
Tel +3292643289 / Fax +3292643575
Email: Marnix.Vanbelleghem@UGent.be

Keywords: moisture experiment, climatic chamber, validation, HAM, CFD, BES

Abstract.

The presence of hygroscopic materials has a large impact on the moisture balance of buildings. Nowadays, HAM (Heat, Air and Moisture) models are widely used to investigate the role of hygroscopic materials on the performance of buildings, i.e. on the building envelope, the indoor climate and valuable objects stored within the building. Recently, these HAM models are being coupled to CFD models to study the moisture exchange between air and porous materials on a local scale (microclimates), or to BES (Building Energy Simulation) models which focus on the interaction between air and porous materials at building level. Validation of these numerical codes is essential to gain confidence in the codes. However, available experimental data are rather scarce.
This paper describes the design of a new test facility for humidity experiments. A dedicated AHU system is used to provide well-controlled air (constant temperature and RH) to an airtight and well-insulated room-size test chamber. In one of the walls of the chamber a calcium silicate sample is installed. A step in RH of the supply air is imposed. Temperature and RH of the supply air, the room air and on various depths inside the sample are continuously registered during the experiments. Two types of experiments were carried out to validate a coupled CFD-HAM model and a coupled BES-HAM model. The temperature outside the test chamber was controlled and there was no temperature difference imposed across the chamber walls. Comparing the models with the measured data gave satisfactory agreement.

1. Introduction

During the last decades an emerging trend exists to design high performance buildings. Energy-efficient buildings should be designed without compromising the indoor comfort level. Both temperature and humidity play an important role in determining the indoor climate in buildings. While the influence of temperature is well-known, several studies have shown that the indoor relative humidity has a severe impact on the perceived indoor air quality [1,2]. Temperature and relative humidity also play an important role in the durability of a building. A lot of damage mechanisms in buildings are triggered by temperature or relative humidity or a combination of both. For example limiting the indoor humidity is indispensable to prevent valuable hygroscopic

objects (e.g. panel paintings) from moisture-related damage [3,4,5]. To ensure the conservation of valuable objects a stable indoor climate is required. Temperature and humidity variations may result in shrinking and expanding of the objects and hence induce mechanical stresses which can lead to damage such as cracks or breaking of the material. Furthermore excessive indoor humidity may lead to condensation and mould growth e.g. at thermal bridges or on windows. These should be avoided as they have an adverse effect on the durability of the building envelope.
Often large, expansive and energy consuming equipment is needed to keep temperature and relative humidity at an acceptable level. For many decades researchers have looked for ways to improve the energy efficiency of buildings without reducing the comfort level. Simonson et al. [2] proved that using hygroscopic building materials can reduce relative humidity and temperature fluctuations. As a result a more stable indoor climate can be provided and the perceived indoor air quality and occupant comfort level can be increased. A study by Osanyintola et al. [6] shows that using hygroscopic materials can reduce the energy use of a building. Similarly, the hygroscopic interaction must be included when evaluating and sizing humidity-controlled HVAC systems in high performance buildings. For instance Steeman et al. and Woloszyn et al. looked at the importance of including the hygrothermal interaction when evaluating indirect evaporative cooling and humidity controlled ventilation systems respectively [7,8].

A good knowledge of the humidity level in rooms and at surfaces is needed. Since buildings are complex systems, they can be studied at different levels (whole buildings, rooms, building components…). Depending on the application, heat, air and moisture transfer in buildings is modelled through different approaches and a lot of different modelling tools are being developed. In the last years, international research projects and researchers focused on a better understanding and prediction of the hygrothermal behaviour of buildings and building envelopes [9]. To understand the phenomena well, numerical tools, i.e. HAM (Heat, Air and Moisture) models, are used. These HAM models allow to simultaneously describe heat and mass transfer in hygroscopic building objects. A good overview of existing HAM models is given in the scope of Annex41 [10] and Annex24 [11].
A new trend in HAM modelling is the coupling of these models to BES (Building Energy Simulation) models or CFD (Computational Fluid Dynamics) models depending on the application aimed at. BES models generally focus on energy use and thermal comfort and predict the relative humidity in a building in a simplified way. They allow for complex building geometries and a relatively short calculation time and are therefore applicable to long term simulations. An integration of HAM allows to include the hygrothermal interaction with the building envelope or furniture in a more detailed way [12,13]. While BES models assume well-mixed indoor air conditions, CFD models are used to calculate 3D temperature and velocity distributions in rooms in a detailed way. By coupling CFD with HAM, 3D local hygrothermal interaction between air and porous surfaces can be studied [4,14,15]. In contrast to BES, these types of models ask for a considerably longer calculation time. They can be applied to predict the local microclimate around valuable objects e.g. around a painting [4] or at the proximity of thermal bridges. To summarize, the coupled CFD-HAM model mainly focuses on object level, while the coupled BES-HAM model describes the hygrothermal conditions of a building.
Note that zonal models, in which the indoor air is subdivided in a smaller number (order of 10 to 100) of computational cells, form the intermediate level between BES and CFD models, and can also be coupled with HAM [16, 17]. This type of model will however not be discussed further in this paper.

In order to gain confidence in the codes and to investigate whether they are able to predict realistic conditions well, validation of these tools is necessary. Although a lot of numerical research has been undertaken with respect to HAM models, experimental campaigns remain rather limited. Many recent works have often focused on numerical and analytical investigations rather than experimental investigations e.g. benchmark cases developed in HAMSTAD project [18] or Annex 41 Common Exercises [10]. There is a need for more experimental data that quantifies HAM transport in porous building materials. To ensure a good validation study, it is important that all input parameters (i.e. boundary conditions, material properties etc.) are well-measured and available, and that influences from surroundings are reduced to a minimum. This is often not the case with field measurements where many external influences are unknown or hard to measure like weather conditions, building occupation… Therefore the experimental work is generally performed in well-controlled conditions, i.e. in climatic chambers or specially built test facilities.

The aim of this paper is three-fold:

(1) **Section 2** summarizes some existing test facilities used for humidity experiments. From this overview, the aspects lacking in humidity experiments can be derived.
(2) **Section 3** discusses both the design of the climatic chamber (test set-up) and the air handling unit used to control the supply air conditions. A detailed description of the applied control strategy is presented. This part continues which the instrumentation and calibration of the sensors in the test chamber. This section should enable other researchers to use the experimental data generated by the test facility for validation of their models. Furthermore, this section allows other researchers to build future test facilities.
(3) It is important to stress that the test facility has been designed for different types of experiments: both for the validation of a coupled CFD-HAM model and for the validation of a coupled BES-HAM model. **Section 4** shows the results of these measurement campaigns respectively.

2. State of the art

Moisture experiments can be roughly classified into room-size moisture buffering experiments, building envelope performance experiments and wind tunnel experiments. In the next sections some of these experiments are discussed.

2.1 Room-size moisture buffering and humidity distribution experiments

In **room-size moisture buffering experiments** generally the response of a test room to the presence of hygrothermal materials is investigated. This type of experiments can be used for validation of existing numerical (BES) tools and to investigate the importance of hygroscopic (finishing) materials on the indoor climate (damping of RH variations). BES models assume well-mixed indoor air, when validating these models it is thus important that this assumption is fulfilled. A differentiation can be made between test rooms located outdoors for which the outdoor conditions (temperature, RH) are measured, and test rooms located in a climatic chamber of which the conditions of temperature and RH can be controlled during the tests. Generally this type of tests aims to mimic the exposure to daily humidity variations, but in a controlled way.

Svennberg et al. [19] investigated the moisture buffering effect of a fully furnished room. The experiments were carried out in a well-insulated and vapour tight test cell (PASSYS cell,

Denmark), consisting of the actual test room and a service room. Furniture and furnishings such as carpet, curtains, a chair, ... were successively introduced into the test room and the RH in the test room was registered when a moisture cycle was imposed. The indoor temperature was kept constant during the experiment. The authors concluded that lightweight materials largely contribute to the moisture buffer capacity of a furnished room. Hedegaard et al. used the same test facility to study the moisture buffer capacity of two types of interior walls (i.e. a cellular concrete wall and a plasterboard construction) both in untreated form and covered with a finish (i.e. an untreated finish or a painted rendering) [20]. During the experiments, the indoor temperature was kept constant while the interior walls were exposed to cyclic humidity variations. The response of the indoor humidity and the moisture content change of a wall component specimen were measured. The results showed that finishes have a large impact on the buffer performance of underlying materials.
In the scope of the research project 'Whole Building Heat Air and Moisture Response' of the International Energy Agency [9], the response of two identical well-insulated and vapour tight rooms was measured under a moisture production and real climatic conditions. These rooms were situated at the Fraunhofer Institute in Holzkirchen (Germany). Inside the test room, the temperature was kept at a constant level. Three cases were distinguished and compared to the reference test room: a vapour tight finishing, gypsum board applied to the walls and gypsum board applied to the walls and the ceiling [10]. The same test facility was used by Holm and Künzel [21] to investigate the moisture buffering of different wood-based finishing materials.
Yang et al. have studied the moisture buffering behaviour of two types of finishing materials (i.e. uncoated gypsum and pine paneling) and of two types of furniture (i.e. a bookshelf with books and a fully furnished room). The experiments were carried out at different ventilation rates and for some cases the RH distribution in the test room was monitored during the experiments [22]. For these tests only the lower room of a two-storey test hut built inside a climatic chamber of which the temperature and humidity were controlled, was used (CBS climate chamber at Concordia University in Montreal, Canada). Additional experiments were performed in which moisture movement through a large horizontal opening between the upper and lower room of the test hut was measured. In these tests the interior surfaces were non-hygroscopic and no furniture was added to the room [10].
Similarly Yoshino et al. [23] (test room Akita university, Japan) have used a room size experiment to look at the moisture buffering in gypsum boards. The actual test room is also located inside a climatic chamber, from which the temperature and humidity can be controlled. Different experiments were carried out with different configurations of gypsum board (e.g. on walls, ceiling, floor) and different ventilation rates (no ventilation, 1ACH and 5ACH). Each experiment consisted of 6hours of humidification followed by 12hours without humidification. During humidification water vapour was produced by evaporating moisture from two water reservoirs. The boundary conditions of the test room, ventilation rate, amount of moisture production, air temperature and humidity were measured and used to validate six numerical HAM models.

On the other hand some **in-situ measurements** were reported in literature. Plathner and Woloszyn [24] experimentally quantified the influence of moisture buffering on the transport of airborne moisture from the kitchen to the other rooms in a fully furnished, unoccupied semi-detached two-storey test house. By comparing the water vapour increase to the concentration increase of an inert tracer gas released simultaneously, moisture buffering in porous surfaces was found to have a large influence on the humidity distribution in the dwelling. Due to the storage capacity of the building envelope and furniture, moisture was absorbed by porous surfaces before reaching the other rooms. During the tests the outdoor climate was registered, as well as the temperature and RH in the centre of each room. The latter were compared to

numerical results. Similar experiments in an unoccupied three-storey house were reported by Oldengarm [25]. These experiments can be used to validate coupled multizone airflow-HAM models, however, no material properties of the furniture were available.
Simonson [26] performed a full scale investigation in a two-storey field test-house in Finland. The house had a well-insulated wooden frame construction without vapour retarder. During the experiments the conditions inside a bedroom with and without hygroscopic finishing were measured while water vapour was generated during the night to mimic the presence of two sleeping adults. Temperature and RH of the outdoor air were registered as well. The results showed that the porous building envelope decreases the peak humidity in the bedroom during the night by up to 20%RH and increases the minimum indoor humidity in the winter by about 10%RH.

All above tests are assumed to be carried out under well-mixed air conditions, which is a necessary assumption for validation of BES models. These well-mixed conditions are generally assured by using a large enough ventilation rate or by using additional fans in the test room, e.g. in [19] and [26]. In these experiments the indoor RH and temperature are generally measured by one or only few sensors at the centre of the test rooms. However, temperature stratification and uneven moisture distribution are prevalent conditions within rooms. Moreover the distribution of RH can vary significantly along interior surfaces, which affects the moisture transfer between the indoor air and the surface material, and as a result, the moisture buffering behaviour of surface materials. Room-size experiments, in which the **humidity distribution inside a room** is measured and which can be used to validate CFD models are rather scarce. The experiments of Yang et al., mentioned earlier, in which the moisture distribution in one room or both test rooms were registered, enable to validate CFD tools [10, 22]. Hohota on the other hand [27], performed detailed experimental investigations on the air velocity, temperature and relative humidity field in a non-hygroscopic test room and used the results to validate a CFD model which takes into account condensation against impermeable surfaces. The experiments were carried out in the MINIBAT test facility (located in Lyon, France), which consists of two identical, adjacent test rooms. One of the rooms is adjacent to a climatic chamber which is used to mimic the outer climate while the temperature of the other wall surfaces is kept constant. The same test facility was used by Teodosiu [28] to predict indoor comfort taking into account the indoor moisture distribution. The results were used to validate a CFD model. In the latter studies [27, 28] the interaction with porous surfaces was not considered.

2.2 Performance of building envelope systems

On the other hand several researchers used a climatic chamber to investigate the **performance of building envelope systems**. In these tests often one of the walls of the climatic chamber was interchangeable (e.g. in [29]) or the test wall is placed between two parts of the climatic chamber of which one part mimics the outer climate and another represents the inner climate (so-called hot box and cold box, e.g. in [30]).
Apart from room-size experiments (see Section 2.1), the CBS climatic chamber at Concordia University was also used for envelope performance investigations (Table 1). Sadauskiene et al. [30] used the test facility to study the effect of an exterior painted thin render finish on the drying rate of exterior-insulated walls in a cold and humid climate. In these tests, the building envelope is positioned in between the hot and cold box representing dynamic indoor and outdoor conditions. Additionally, an amount of moisture could enter the construction system by means of an artificial rain poured on the surface of the walls. Fazio et al. [31] gives a detailed description of how the test-set up can be used for envelope component performance testing. The same test facility was used by Alturkistani [29] to investigate the drying capacity of different envelope configurations. In

contrast to Ref. [30], here the envelope of the two-storey test house built inside the climatic chamber was tested. In the experiments, the moisture contents of the materials in the assemblies were monitored by gravimetric samples which were cut out from sheathing and stud materials. The same set-up was used by Li et al. [32] for validation of a 2D HAM model. In these experiments measured and calculated moisture content profiles on sheathing are compared for different types of wall panels.
Pavlik et al. [33,34] designed a system of climate chambers for the simulation of external and internal climatic conditions (NONSTAT). A studied envelope structure was placed in a connecting tunnel between two climate chambers. In one chamber outside conditions were simulated, in the other inside conditions were imposed. In the tested structure the moisture content, relative humidity and temperature was monitored.
Vici et al. [35] used climatic chamber experiments to look at the behaviour of wooden boards, which represented the supports of panel paintings, subjected to cyclic humidity cycles. No detailed information about the test facility was included in the paper. Belarbi et al. [36] performed 1D and 2D experiments on lime-cement mortar and sandstone for the validation of a 2D HAM model. The experiments were carried out in a modified oven inside a climatic chamber from which the temperature and RH were controlled. Both the temperature and RH in the climatic chamber, the surface temperature and the temperature and moisture ratio distribution inside the sample were measured.

2.3 Wind tunnel experiments – convection coefficient experiments

The convective mass transfer coefficient is an important parameter because it is a measure of the resistance to mass transfer between flowing air and porous surfaces and therefore has an impact on the moisture buffering behaviour of hygroscopic materials. Since these mass transfer coefficients are difficult to determine experimentally, often convective heat transfer coefficients are measured and the analogy between heat and mass transfer is used to determine the convective mass transfer coefficient [37].

Recently, **wind tunnel experiments** were performed in the transient moisture transfer (TMT) facility which was designed to study 1D heat and moisture transfer between a flowing air stream and a porous material and is located at the University of Saskatchewan, Canada. A good description of the test facility is given in Talukdar et al. [38]. In the experiments a small converging wind tunnel produces a steady, fully developed air flow at varying velocities, temperatures and RH's, above the surface of a porous material. Two hygroscopic building material samples (i.e. cellulose insulation and spruce plywood), of which the hygrothermal properties were measured, were used. During the tests the changes in mass, relative humidity and temperature were measured at different depths inside the samples. For both material samples three different types of tests were performed: (1) a single step change in humidity (from 50%RH to 85%RH), (2) different flow rates resulting in a laminar and turbulent flow and (3) cyclical tests for which a RH of 75% imposed for two days is followed by a RH of 33% for two days [39]. Olutimayin et al. [40] applied the same test facility to study the vapour boundary layer in a bed of cellulose insulation following a step change in ambient humidity. Both an isothermal test and a non-isothermal test were performed. The experimental data are used for verification of a mathematical model. Osanyintola et al. [6, 41] used both the TMT test facility and a sealed glass jar facility to determine the moisture buffer capacity (MBC) of spruce plywood, which can be used to quantify the potential for hygroscopic materials to damp indoor humidity variations. Due to differences in boundary conditions and to a different sample size of the plywood, MBC differences

up to 18% are registered. The experimental data were furthermore used to validate a numerical model.

To determine the convective mass transfer coefficients at the porous surface, experiments based on the adiabatic evaporation of water from a tray located in the lower panel of a horizontal rectangular duct were carried out e.g. by Iskra et al. [42]. In these tests both the evaporation rate from the tray of water and the vapour density difference between the air stream and the surface of water are measured. The vapour density of the air stream is determined from the measured temperature and RH of the airstream while the vapour density at the surface is based on the measured water temperature and the saturated air assumption. Talukdar et al. used the results of similar experiments for comparison with CFD simulations [43].
On the other hand Bednar and Dreyer [44] reported on detailed in situ investigations on realistic mass transfer coefficients in a test room (room area 13.4m² and height 3.5m) where different heat and moisture production and/or ventilation strategies were applied. By measuring the mass loss of a small insulated specimen (32cm³), the surface temperature in the centre of the specimen and the temperature and RH of the air close to the specimen, mass transfer coefficients could be determined.

2.4 Discussion

Above literature review has revealed that a lack of experimental data exists especially for the validation of coupled CFD-HAM models. The existing facilities focus on the determination of transfer coefficients [38] or on the concentration pattern in the room [27]. Since the experiments by Talukdar et al. [38] were performed in a wind tunnel, it was not clear whether the measurements correspond well to realistic cases.
On the other hand, more data are available with respect to validation of multizone models. At this point it must be noted that in some experimental campaigns not all input data necessary for numerical tools were available, e.g. material properties [19].

Some important points of interest were considered when designing the new test facility: firstly the new test facility wants to generate more realistic flow patterns typically encountered in buildings instead of fully developed laminar or turbulent air flow conditions encountered in Ref. [38]. The innovative part of the new test-facility consists of the fact that a porous sample is installed in one of the walls of the test room and is smoothly aligned with the test wall in which it is positioned. The air jet blows directly on the sample and mimics the interaction between the indoor air and a porous wall surface.
Furthermore the temperature and relative humidity distributions inside the porous material sample are measured during the experiments, together with the air flow patterns around the material. This is new for experiments on room-scale and allows to validate a coupled CFD-HAM model. This will be further discussed in **Section 4.2**. Another important point is the flexibility of the test facility. By adding additional hygroscopic material to the test room, the experimental set-up allows to validate coupled BES-HAM models in which the indoor air in the test room is well-mixed. This will be discussed in **Section 4.3**.

3. Climate chamber design

The lay-out of the new test facility will be extensively described in the next sections. First the design of the test chamber will be discussed in **Section 3.1**. After, **Section 3.2** and **3.3** focus on the air handling unit and the instrumentation of the test facility respectively. Finally, the test sample is discussed in **Section 3.4**.

3.1 Test chamber

The test facility was built at the laboratory of the Department of Flow, Heat and Combustion Mechanics at Ghent University (www.floheacom.ugent.be) and consists of an outer and an inner chamber. The outer chamber is mainly used to minimize effects from the surroundings, for instance day/night temperature fluctuations. Similar to for instance the Atika test room [23], the inner chamber is the actual test chamber. It represents a small room measuring 1.8m in width, 1.89m in depth and 1.8m in height (volume 6.12m^3). The outer room measures 3.0m width on 2.7m depth and has a height of 2.4m. The test facility is schematically represented in Figure1, a view on the test room is shown in Figure 2. The wall panels (type ISOCAB [45]) of the inner and outer room consist of 6cm rigid high density polyurethane foam with a thermal conductivity of 0.0223 W/m·K, sprayed in between two skins of white polyester lacquered, galvanized steel plate (thickness 0.63mm). The panels have an overall U-value of 0.372 W/m^{2}K according to the manufacturer [46]. The floor consists of multiplex panels with a phenol anti-slip surface reinforced with glass fibre. Its thermal conductivity is 0.366 W/m·K. The wall opposite to the air inlet is a test wall, consisting of 6cm mineral wool (λ~0.04W/m·K) in a timber frame. A calcium silicate sample is positioned in the test wall. This test sample is discussed more in detail in Section 3.4.

Note that in order to minimize the heat losses to the outer room, a small heating device (i.e. a light bulb) was placed in the outer chamber. The light bulb turns on if the temperature in the outer room is below 25°C.

3.2 Air handling unit

A closed-looped air handling unit (AHU) draws air from the inner room with a recirculation fan. The ventilation air inlet and outlet are positioned respectively at the top and bottom of the wall opposite to the test wall, as indicated in Figure 1. Temperature, relative humidity and velocity of the entering air jet are closely controlled with a dedicated air conditioning system. The air is successively cooled and dehumidified by a cooling coil (with a maximum cooling capacity of 3.5kW). When the air reaches its dew point, condensation starts and the humidity ratio of the air drops. The air at lowered temperature passes through a heat exchanger where a resistive heater heats up the air to the desired temperature. By heating the air, its relative humidity drops. Steam is then added to the dry air to humidify the air to the required relative humidity set point (Figure 1). The steam humidifier works as follows: a dosing pump supplies a heated cylinder with demineralised water. The cylinder is kept at a high temperature (± 300°C) by a resistance wire that is wrapped around the cylinder. The water that enters the cylinder immediately evaporates when it comes in contact with the hot cylinder wall. This way the time delay between the moment the liquid water enters the cylinder and the moment this water leaves the cylinder as steam is minimal. The dosing pump has a manually adjustable stroke length and the rotation speed is controllable. With a maximum of 180 rpm (revolutions per minute) and a stroke volume of up to 0.13ml this results in a maximum flow rate of 1.4 litres per hour. The produced steam is then

injected into the air duct. Contact of the steam with colder duct walls must be kept to a minimum to avoid condensation.
The air then passes through a buffer vessel with a volume of 25 litres. The buffer vessel is placed not far from the steam injection point in the air circuit to ensure a good mixture of the water vapour in the air. This buffer vessel levels out the relative humidity fluctuations caused by the humidification system and damps out temperature fluctuations. Finally a flow straightener ensures a fully developed flow pattern when the air enters the climate chamber.

A constant inlet air velocity is guaranteed by a fan with a constant rotation speed. The air change rate can vary between 0ACH and 10ACH, corresponding to a maximum air flow rate of about 61.2m^3/h (mass flow rate of 68 ± 2 kg/hr). The airtightness of both the inner room and the AHU-circuit was verified with a CO_2 tracer gas decay experiment. During the tracer gas measurements, the air change rate was set to its maximum value (approximately 10ACH). An infiltration rate of 0.033ACH was measured, which proves a satisfactory airtightness of the test room.

During operation of the test room, the temperature and the relative humidity at the air inlet of the test chamber need to be controlled closely. The applied control strategy for temperature and relative humidity is shown on Figure 3: a control loop for temperature and a control loop for relative humidity can be distinguished. Both temperature and relative humidity are measured at the chamber inlet (indicated in Figure 1). These measured values are compared with the corresponding set points. The difference between set point and measured value then serves as an input for the PID controller which steers the resistive heater for temperature control and steers the pump of the humidifier by adjusting its rotation speed for humidity control. G11, G12 and G22 on Figure 3 represent the transfer functions of the system.

The system is a multiple-input-multiple-output system (MIMO), which means that the two control loops cannot be entirely separated. This may render a smooth temperature and relative humidity control rather difficult. Changes in temperature change the relative humidity when the absolute humidity remains unchanged. On the other hand the hot steam added to the air flow influences the air temperature. The temperature loop has a smaller time constant than the relative humidity loop. Therefore the influence of the relative humidity on the temperature is small and can be neglected. The influence of the temperature on the relative humidity on the other hand (represented by G12) cannot be neglected due to the slow time response. This was also concluded by Huang et al. [46]. This will be further discussed in the following section (see Figure 4).

3.3 Instrumentation

The relative humidity at the inlet of the chamber is measured by a capacitive humidity sensor TRANSMICOR T232 from GEFRAN. This sensor has an accuracy of ±2% between 5%RH and 95%RH. The relative humidity in the test room and in the test sample is measured with capacitance RH sensors (type HIH-4000 humidity sensors from Honeywell). Thermocouples type K are used to measure the inlet air temperature, the temperature in the centre of the test room, the temperature at different depths in the calcium silicate sample, near the front and back surface of the test sample and against the walls of the test room (indicated by a-d in Figure 10b). All sensor signals are read by a voltage scanner and the measured values are then sent to a computer where they are stored. All data are recorded every ±3s during the experiment.

a. Response of the RH sensors

As mentioned in the previous section, a fast response of the temperature and relative humidity is essential. To evaluate the response time of the control system (and hence the performance of the controllers), two tests were conducted. Figure 4a shows the response of the relative humidity at the inlet of the chamber when the set point is altered from 50%RH to 65%RH and then back to 50%RH. During the test, the temperature of the supply air is kept constant at 25°C. Hardly any influence of the step change RH on temperature is noted in Figure 4a. Hence, when temperature stays constant, the response of the sensors is in the order of seconds or even less and an immediate change in relative humidity is noted.
On the other hand Figure 4b shows that when the temperature changes with a constant absolute humidity, the response of the RH sensor is much slower. The response time grows tremendously when the air temperature decreases from 25°C to 20°C and then back to 25°C. A response time up to ten minutes is measured. This is in correspondence with Dooley et al. [47] who came to the same conclusions. As a result, experiments with a varying supply air temperature are difficult to perform.

b. Calibration of the temperature and RH sensors

To obtain good and reliable measurements in the climatic chamber, a precise calibration of the sensors used in the test chamber is indispensable. To calibrate the thermocouples a dry block calibrator was used. This method allows to calibrate thermocouples to an accuracy of ±0.1°C.
To calibrate RH sensors, generally saturated salt solutions are used. These solutions decrease the relative humidity in the atmosphere of a closed (glass) jar to a relative humidity below 100%. The equilibrium relative humidity is known for a number of saturated salt solutions, their equilibrium relative humidity furthermore depends on temperature. This equilibrium relative humidity can then be used as a reference point for calibration of the RH sensors. One disadvantage of this technique is the strong dependence on temperature: small fluctuations of the temperature of the surroundings change the equilibrium relative humidity of the salts. As a result, calibration of the sensors must be performed in a controlled environment, e.g. in a climatic room. Furthermore, a relatively long period is required before the saturated salt solution reaches an equilibrium state.

To overcome some of these drawbacks, a new calibration procedure was developed. The new method allows both to facilitate the existing procedure and yet to obtain a precise calibration of the RH sensors. In this procedure saturated salt solutions are placed inside a glass box and a chilled mirror is used to determine the dew point in the box with an accuracy of ± 0.2°C. At the same time, the dry bulb temperature in the box is measured. The relative humidity in the box can now be determined from the measured dew point and the measured air temperature. By consequence, the salt solutions are only used to create a certain atmosphere in this procedure ($MgCl_2$(33%RH), KCO_3(43%RH), NaBr(59%RH), NaCl(75%RH)). As a result, the saturated salt solution does not necessarily need to reach equilibrium conditions and the test can be performed much quicker. Another benefit of the new test procedure is that the tests become less sensitive to the temperature of the surroundings. The new procedure allows to calibrate the RH sensors with an accuracy of ±1.4%RH.
Additionally, one of the RH sensors was calibrated in a so-called two-pressure calibrator. This method allows to very precisely calibrate RH sensors. In this method air or nitrogen with water vapour is saturated at a known temperature and pressure. The saturated high-pressure air flows from the saturator, through a pressure reducing valve, where the air is isothermally reduced to

test pressure at test temperature. When equilibrium is reached, the resulting air RH can be determined by measuring the temperature and pressure in the saturator, and the test temperature and test pressure after pressure reduction. A comparison between the two-pressure method and the newly developed procedure shows good agreement between both calibration methods (Figure 5).

3.4 Test sample

In the test wall a calcium silicate sample is positioned (20cm x 20cm, thickness 10cm). The test sample is placed directly opposite to the air inlet of the test room. Figure 6a represents a section of the test sample; Figure 6b shows a front view of the calcium silicate sample in the test wall. The sample is sliced into four layers of respectively 10mm, 15mm, 25mm and 50mm thickness. Between each two material layers, in the middle, a thermocouple and a small capacitance relative humidity sensor made by Honeywell are placed. The positions of the thermocouples and relative humidity sensors are indicated in Figure 6a. The layers are then pressed back together to ensure good contact. In section 4.1 the results of a preliminary tests which showed the possible impact of the sensors on the measured temperature and RH in the sample, are given. The test sample is placed in a plexiglass box. The four sides and the back side are sealed with paraffin to avoid moisture exchange. At the sides and the back the sample is insulated with 4cm mineral wool to avoid heat exchange with the surroundings. These measures should ensure 1D moisture transport in the material sample.

The calcium silicate used in the tests is a highly hygroscopic material which renders it suitable to use in the validation experiments of a coupled CFD-HAM model or a coupled BES-HAM model. The material properties of the calcium silicate were extensively measured by different laboratories during the HAMSTAD-project (Heat, Air and Moisture Standards Development) [48,49]. In the calcium silicate material a fine and a coarse pore system were distinguished. The measurements showed an open porosity ψ_0 ranging from 84% to 90%. The open porosity ψ_0 is defined as the ratio between the pore volume open for moisture transport and the total volume of the material sample. The material properties measured by the KU Leuven laboratory were used in the validation study and are given in Table 1. A dry vapour resistance factor of 5.42 and a dry thermal conductivity of 0.06W/m·K were registered. It was found from sensitivity analysis [50] that the measured value of 5.42 for the vapour resistance was too high and not in correspondence with measurements by other laboratories. Therefore a value of 3 was used. The measured saturation moisture content w_{sat} was 894kg/m^3.

4 Validation experiments

Two types of validation experiments can be distinguished. The experiments can be either used for validation of a coupled CFD-HAM model or a coupled BES-HAM model. In the following sections, both types of validation experiments will be described in detail. Furthermore, numerical results obtained with a CFD-HAM model and a BES-HAM model will be compared with measured data from the climatic chamber experiments. First, the results of a preliminary experiment are shown to confirm the performance and the repeatability of the newly developed test set-up.

4.1 Preliminary experiment: effect of sample cutting

Preliminary experiments were carried out to check whether sample cutting may have an effect on the temperature and relative humidity profiles which are measured on different depths in the sample. Due to cutting of the calcium silicate sample at the different positions (at 10mm, 25mm and 50mm) for the installation of a thermocouple and a relative humidity sensor, it is possible that small air layers arise in between the different material parts when the sample is assembled again. Because of this, the material properties may no longer be homogeneous along the depth of the material, which can affect the overall permeability and sorption of the sample. In turn this may influence the temperature and relative humidity profiles measured inside the sample. To check the possible effect of the cutting edges in the sample, a new sample is prepared which is only sliced at 25mm depth. In this material sample the influence of a possible air layer at 10mm depth is hence excluded. Both samples are successively installed in the test wall and with each sample an identical experiment is performed. Before each experiment the calcium silicate sample is preconditioned for four days by supplying air (10ACH) at 25°C and 50% relative humidity until the temperature and relative humidity differences inside the sample are below the uncertainty interval of the sensors (i.e. ±0.1°C and ±1.4%RH). During the experiment the supply air temperature is kept at 25°C, while a relative humidity step is imposed from 50% to 70%: 8 hours of high relative humidity (70%) are followed by 16 hours of low relative humidity (50%). This cycle is repeated five times. Apart from the calcium silicate sample in the test wall no other porous material is present in the room. Figure 7 compares the measured temperature and relative humidity profile at 25mm for the last three cycles. Note that the latent heat of evaporation has a strong effect on the temperatures inside the sample: the temperature in the sample rises if water vapour is absorbed by the sample, a temperature decrease is noted when water vapour is released from the sample. The relative humidity measured at 25mm in both samples is quasi identical. Also the associated temperature measured in the sample is comparable, in the third cycle a difference of about 0.2°C is noted.
The temperature and relative humidity course at the front and the back side of the sample show that in both experiments the boundary conditions are similar (Fig. 7b and Fig. 7c). At the front side of the sample, the relative humidity between the two tests differs from 0.5%RH up to 1.4%RH when the relative humidity of the supply air is 70%. The maximum difference between the temperatures measured at the front side is 0.1°C. At the back side, the average difference in relative humidity is smaller than 0.5%RH while the maximum temperature difference is about 0.2°C. Note that the thermocouple and relative humidity sensor at the front and back side of the sample do not exactly register the conditions at the sample surface but rather measure the temperature in a small air layer near the surface. These measurements show that the boundaries in both cases are the same. Consequently, the experiments demonstrate that the cutting edges do not have a considerable effect on the temperature and relative humidity profile measured in the sample. Furthermore the experiments have shown to be reproducible.

4.2 Experimental validation of a CFD-HAM model

In the first type of experiments, a jet is created which blows on the calcium silicate sample in the test wall. During the experiment the temperature, air speed and relative humidity of the jet are closely controlled. The temperature and relative humidity response at different depths (i.e. 10mm, 25mm and 50mm) inside the test sample is measured when a step in relative humidity is imposed to the inlet air. On the other hand, the inlet air temperature is kept at a constant value.

Before the experiment the calcium silicate sample is preconditioned for four days by supplying air (10ACH) at 25°C and 50% relative humidity until the temperature and relative humidity differences inside the sample are below the uncertainty interval of the sensors (i.e. ±0.1°C and

±1.4%RH). During the experiment the supply air temperature is kept at 25°C, while a relative humidity step is imposed from 50% to 70%: 8 hours of high relative humidity (70%) are followed by 16 hours of low relative humidity (50%). This cycle is repeated five times. Apart from the calcium silicate sample in the test wall no other porous material is present in the room. A 2D hotwire anemometer is used to measure the velocity field inside the test room. The anemometer is connected to a robot arm which is controlled by a computer. The robot arm can move in two directions, allowing measurements in the vertical plane of the jet (Figure 8).

These measurements are used to validate a coupled CFD-HAM model. The CFD-HAM model computes the water vapour transport in the hygroscopic material as well as in the surrounding air. An internal coupling approach is used where both the porous material domain and the air domain are solved within the same solver. As a result there is no need for mass transfer coefficients to couple the mass transport between both domains [51]. In a more classical approach, HAM models use transfer coefficients to link the transport in the porous material with transport in the surrounding air. These transfer coefficients are often derived from correlation and are strongly dependent on the air velocity. Therefore a good knowledge of this air velocity is important when an accurate estimation of the transfer coefficients is needed. On the other hand, correlations for transfer coefficients found in literature are often only applicable for certain cases. This implies that a good estimation of these transfer coefficients is difficult. The CFD-HAM model used here overcomes these issues by avoiding the use of these coefficients.
The coupled CFD-HAM model was preliminary verified and a sensitivity study was performed, for more details on the model and the implemented equations the reader is referred to [4] and [52]. In this paper only the governing equations for heat and moisture transport in the air and porous material are shown.

The air is modelled as an incompressible ideal gas. In this case the energy and moisture transport equations reduce to equations (1) and (2).

$$\frac{\partial}{\partial t}\left(\rho_{air} CT\right) + \nabla.\left(\vec{v}\rho_{air} CT\right) = \nabla.\left(\lambda_{air}\nabla\left(T\right) - \left(C_{vap} - C_{air}\right)\vec{g}T\right) \quad (1)$$

$$\frac{\partial}{\partial t}\left(\rho_{air} Y\right) + \nabla.\left(\rho_{air}\vec{v}Y\right) = \nabla.\left(\rho_{air} D\nabla\left(Y\right)\right) = -\nabla.\vec{g} \quad (2)$$

with

$$C = YC_{vap} + \left(1 - Y\right)C_{air} \quad (3)$$

In these equations ρ_{air} [kg/m³] is the density of the humid air, C_{vap} [J/kg·K] is the specific heat capacity of water vapour, C_{air} [J/kg·K] is the specific heat capacity of air and C [J/kg·K] is the weighted average specific heat capacity according to equation (3), λ_{air} [W/m·K] is the thermal conductivity of air and g [kg/m²·s] the water vapour diffusion flux. D [m²/s] is the diffusion coefficient of water vapour in air. T is the temperature [°C] and Y [kg/kg] the mass fraction of water vapour in the air. The first term on the left hand side of each transport equation is the storage term, the second term represents the convective term while the right hand side represents the transport by diffusion.

For the porous material zone the following assumptions are made in the model:

- No air transfer occurs

- Liquid transfer is not dominant
- Moisture storage only depends on relative humidity
- The temperature remains below the boiling point
- There is no radiative transfer inside the porous material

The model is only valid in the hygroscopic range (RH <98%). Here moisture transfer by equivalent vapour diffusion is dominant. This implies that the moisture transfer can be modelled by a single water vapour diffusion coefficient. Equations (4) and (5) describe the moisture transfer and the heat transfer in the porous material.

$$\frac{dw}{dt} = -\nabla.\vec{g} \Leftrightarrow \frac{\partial w}{\partial RH}\frac{\partial RH}{\partial Y}\frac{\partial Y}{\partial t} + \frac{\partial w}{\partial RH}\frac{\partial RH}{\partial T}\frac{\partial T}{\partial t} = \nabla\left(\rho_{air}\frac{D}{\mu}\nabla(Y)\right) \tag{4}$$

$$\frac{dE}{dt} = \nabla.\left(\lambda_{mat}\nabla(T) - \left(\left(C_{vap} - C_{air}\right)T + L_{vap}\right)\vec{g}\right) \Leftrightarrow$$

$$\rho_{mat}C\frac{\partial T}{\partial t} + C_{liq}T\frac{\partial w_{liq}}{\partial t} + \left(C_{vap}T + L_{vap}\right)\frac{\partial w_{vap}}{\partial t} = \nabla.\left(\lambda_{mat}\nabla(T) - \left(\left(C_{vap} - C_{air}\right)T + L_{vap}\right)\vec{g}\right) \tag{5}$$

with

$$E = \rho_{mat}C_{mat}T + C_{liq}w_{liq}T + \left(C_{vap}T + L_{vap}\right)w_{vap} \tag{6}$$

$$C = C_{mat} + \frac{C_{liq}w_{liq}}{\rho_{mat}} + \frac{C_{vap}w_{vap}}{\rho_{mat}} \tag{7}$$

$$w_{liq} = \frac{\psi_0 - \frac{w}{\rho_{vap}}}{\frac{1}{\rho_{liq}} - \frac{1}{\rho_{vap}}} \tag{8}$$

$$w_{vap} = \frac{\frac{w}{\rho_{liq}} - \psi_0}{\frac{1}{\rho_{liq}} - \frac{1}{\rho_{vap}}} \tag{9}$$

In equations (4) to (9) *mat* refers to the dry material properties, *liq* stands for liquid water and *vap* for water vapour. In the material model described by equations (4) to (9) the following material properties have to be known: the sorption isotherm which states the relation between the equilibrium moisture content w [kg/m³] and the relative humidity RH, the vapour resistance factor μ [-] as a function of moisture content, the dry density ρ_{mat} [kg/m³], the heat capacity C_{mat} [J/kg·K], the open porosity ψ_0 [-] and the thermal conductivity λ [W/m·K]. The liquid moisture content w_{liq} and the water vapour content w_{vap} in the porous material can be related to the total moisture content w through equations (8) and (9) taking into account that $w = w_{liq} + w_{vap}$ and $\psi_0 = w_{liq}/\rho_{liq} + w_{vap}/\rho_{vap}$.

A commercial CFD package (Fluent®) was used to simulate the climate chamber. A 3D structured rectangular grid with 138708 elements was used to discretize the chamber and calcium silicate sample. A grid independency study was performed by comparing the results of the coarse grid with a refined grid of 1109664 cells (two times finer in every direction). When comparing the calculated velocity for both grids, deviations up to 7% were found. Previous studies showed that the velocity near a hygroscopic sample has only a small influence on the heat and moisture transfer in the sample, so it was concluded that using the coarser grid would result in sufficient accuracy.
For simplicity a constant inlet velocity of 10m/s was chosen with a turbulence intensity of 5%. The walls of the chamber are assumed adiabatic except for the back walls of the test sample. Here a constant temperature of 25.4°C is assumed. This value corresponds with the measured temperature at the back of the sample and gave the best results for the simulations.
The incompressible ideal gas law was used to calculate the density. Constant values for the dynamic viscosity, thermal conductivity and mass diffusivity were used. As the interest of the study lies in the heat and mass transfer to the wall (the calcium silicate sample), it is important that the near wall behaviour of the flow is correctly represented. A sufficient refined grid is used near the wall ($y+ <4$) in combination with a k-ω LRN turbulence model. This turbulence model is known to perform well close to walls. A second order upwind scheme is used for the discretization of the convective terms in the transport equations in order to reduce numerical diffusion. The SIMPLE algorithm is used for the pressure-velocity coupling. A double precision representation of real numbers is used to reduce round-off errors.

The transient hygrothermal behaviour of a system consisting of air in contact with a porous material is dominated by the response of the porous material. As the characteristic time scale of heat and moisture transfer in the air is in the order of seconds while the time scale characterizing the hygrothermal response of the porous material is in the order of minutes or hours, the air response can be described as quasi steady state [53]. In other words, the transient hygrothermal behaviour of the air is caused by the varying boundary conditions at the interface with the porous material and at each time step the air can be considered in equilibrium with the new boundary conditions. This does not imply that the air flow cannot feature unsteady phenomena (such as vortex shedding), yet these phenomena appear at a time scale much smaller than the time scale of the heat and moisture transfer we are interested in and do not need to be captured. The time step for the coupled CFD-HAM simulation can thus be chosen based on the characteristic time scale for heat and moisture transfer in the porous material. As the transport equations in both the air and the porous material are solved in the same solver, this time step is used for both media. The airflow is hence also modelled as unsteady. However, because the time step is that large compared to the characteristic time scale in the air, the unsteady term in the heat and mass transport equations becomes negligible compared to the convective term and the equations reduces to a quasi-steady form. For the transient simulations performed in this study a time step of 60 seconds was chosen. The effect of the time step size is evaluated by performing a simulation with a time step of 30 seconds. No appreciable effect was found.

Figure 8 shows the comparison between the measured velocity field in the middle of the chamber and the simulated velocity. A good agreement between both is found. However, the jet shown in Figure 8b is calculated under steady conditions. As mentioned earlier, in reality the jet will experience unsteady phenomena. Because this small time dependency of the jet has no influence on the heat and moisture transport to the porous material, the jet is solved quasi steady state. Small deviations between the measured and simulated jet can thus be attributed to the time dependency of the jet, but this does not affect the results for humidity and temperature in the test

sample. Also, mass transfer between the air and the porous materials is dominated by the vapour diffusion resistance and not by the mass transfer coefficient when the velocity is high enough (forced convection). This implies that a wrong estimation of the velocity near the material or indirectly a wrong estimation of the mass transfer coefficient has little effect on the mass transfer. Note that this is only valid for cases with forced convection. For very low air velocity, where buoyancy driven flow becomes important, the vapour diffusion resistance is no longer dominant. Here the driving forces for airflow are temperature gradients and to a smaller extent humidity gradients. This means that the airflow and by consequence the transfer coefficient depend on the air temperature and relative humidity. More details on this matter are found in [14,51].

Figure 9 shows a comparison of the measured and simulated relative humidity and temperature at three depths in the calcium silicate sample. The material properties of the calcium silicate used in this study are listed in Table 1. This comparison shows a good agreement between measurement and simulations at a depth of 10mm. Deeper in the material (at 25mm and 50mm) the deviations are more pronounced. Several explanations for these deviations can be found. First the exact location of the sensors in the material will have an effect on the measurement results. Secondly the exact boundary conditions are of great importance and finally the input data of material properties can have a severe impact on the simulation results. All of this is discussed in more detail below.

Figure 9c shows the relative humidity in the sample at a depth of 25mm. Three simulation curves are shown together with the measured data (including the error bars). In green the simulation results at exactly 25mm are shown. The dashed lines in red and blue show the simulation results at a slightly different position in the material. The red dashed lines are the simulated values at a depth of 23.2mm (1.8mm less deep in the material); the blue dashed lines are the simulation results at a depth of 26.6mm (1.6mm deeper in the material). During adsorption there is a clear underestimation of the relative humidity. However slight changes in the position of the sensor will results in a higher or lower relative humidity measured in the material. It is not unlikely that the exact location of the sensor in the material deviates from the assumed 25mm, since the sensor has a thickness of 2mm. Figure 9c clearly shows the effect of the sensor positioning. A sensor position at 23.3mm would result in a better agreement of the simulations with the measurements. Changing the position of the sensor in the order of 2mm has only little effect on the simulated temperature (Figure 9d).
The temperature difference between measurements and simulations during desorption at a depth of 25mm (and also to a lesser extent at 10mm) can be attributed to an underestimation of the boundary conditions during desorption. It is assumed that the temperature of the incoming air is constant at 25°C. However in reality there is an uncertainty on this value of ±0.1°C. A change in the incoming air temperature has a direct effect on the temperature in the sample. In other words, an increase of 0.1°C of the incoming air during desorption would result in an increase of the simulated temperature and thus a better fit with the measurements. This was also shown in [52] where the sensitivity of the simulation on changes in boundary conditions was studied. Deeper in the porous material (at 50mm) the effect of inlet air temperature is less pronounced since here the temperature is more determined by the temperature at the back of the sample (which was at 25.4°C).
The largest discrepancies between model and measurements are found at a depth of 50mm. Although a good agreement for temperature is found, the relative humidity differs op to 4%RH. This difference can no longer be attributed to sensor positioning and boundary conditions solely. Previous studies [50,52] showed that besides boundary conditions also material input data can have a severe impact on the modelling outcome. Wrong estimations of this data (especially

sorption isotherm and vapour resistance factor) becomes more important deeper in the material as these effects accumulate.
For most porous materials there is no unique relationship between moisture content and the relative humidity because hysteresis occurs during the adsorption/desorption process. The material will behave differently during adsorption and desorption. Since for this study an adsorption phase is followed by a desorption phase, hysteresis might become important. However in this modelling approach no hysteresis model was implemented. A previous study [52] showed that hysteresis during desorption has a similar effect as using a sorption isotherm with lower moisture capacity ($\partial w/\partial RH$). In other words, the moisture capacity during desorption is lower. It was concluded that the model error due to the lack of a hysteresis model was of the same magnitude as the error due to an inaccurate sorption isotherm.
It is clear that measuring and modelling moisture transport in porous materials in difficult since there are so many parameters involved. It is in fact a combination of uncertainties on different factors (sensor position, boundary conditions, material properties) that result in a deviation between measurements and simulations. Bearing all this in mind, it can still be concluded that there is an overall rather good agreement for the coupled CFD-HAM model with the measurements.

4.3 Experimental validation of a BES-HAM model

This section discusses the room size buffer experiments which are carried out in the test room. This type of measurements can be used to validate a coupled BES-HAM model. In these tests, air at a predetermined temperature and relative humidity enters the room at a controlled flow rate and the response of the test room to humidity variations of the supply air is investigated. Apart from the calcium silicate sample in the test wall, four additional calcium silicate plates (with each average dimensions 950x700x100mm^3) are placed in the test room. The plates are sealed at the four sides with moisture proof tape to ensure 1D vapour diffusion in the plates and have a total exposed area of approximately 5.2m^2. Figure 10 shows a view on the plates in the test room (a) and a schematic representation of the layout of the plates (b). In a preliminary experiment logger (type HOBO with an accuracy of ±3%RH and ±0.2°C) sensors were placed at different positions in the test room and the results showed that an air flow rate of 5ACH and 10ACH was large enough to ensure well-mixed conditions in the test room.

Beforehand the calcium silicate plates were preconditioned in the test room for four days at 25°C and 50%RH. The measured temperature and the relative humidity on different depths in the test sample were used to determine when the calcium silicate plates were in equilibrium with the ventilation air (measured differences below the uncertainty error of the thermocouples and relative humidity sensors). During the actual experiment a supply air change rate of 5ACH is considered and the temperature of the ventilation supply air is kept at 25°C while a step change in relative humidity is imposed from 50% to 70% for 2h each. This cycle is repeated several times.
In the middle of the test room a thermocouple and a small capacitance relative humidity sensor are placed to measure the room conditions (accuracy ±0.1°C and ±1.4%RH). During the experiment, thermocouples are placed against the inside and outside surface of the side walls of the test chamber, as indicated by positions a and d in Fig. 10b, to control the boundary conditions of the inner room. Additionally, temperature and RH at different depths in the test sample were monitored. Also the supply air conditions (i.e. temperature, relative humidity and mass flow rate) are well registered during the test.

Previously these experiments were used to validate a coupled BES-HAM model. Figure 11 shows one of the results of the validation study for three RH cycles. The experiments showed that the calcium silicate plates were clearly able to damp relative humidity variations in the test room. The average RH amplitude in a non-hygroscopic test room was 17.1%RH, compared to 13.6%RH when moisture exchange with calcium silicate plates and the test sample was possible. Furthermore, the experiments clearly showed the latent effect of moisture buffering on the measured temperature in the test room. When the relative humidity in the test room increases to 70% the calcium silicate plates start to absorb water vapour, which coincides with release of latent heat. A clear increase of the temperature measured in the test room is noted. When the relative humidity of the supply air drops to 50%, the plates start to release water vapour to the room air. This is clearly associated with an uptake of latent heat. As a result, the temperature in the test room varies between 25.1°C and 25.7°C.

Figure 11 shows a good agreement between the measured and predicted temperature and relative humidity in the test room. The amplitude of the relative humidity variations in the test room is slightly underpredicted by the model. Maximum relative humidity values are predicted well, but the lower values are underestimated by the calculations. On the other hand the predicted temperature variations are well within the uncertainty interval and a good agreement with the measured data can be observed. A sensitivity analysis carried out to investigate the deviations between the measured and calculated values showed that the differences were mainly attributed to uncertainties to the moisture related material properties (mainly by an overestimation of the vapour resistance factor) [50]. In the same study, the measured and calculated temperature and relative humidity at different depths in the test sample were also compared. For more details on the coupled BES-HAM model, the boundary conditions used and the HAM discretization, the reader is referred to [50].

5 Conclusions

A thorough literature study revealed a lack of well documented experimental data for the validation of coupled BES-HAM model on the one hand and coupled CFD-HAM models on the other hand. Therefore a new test setup was designed and tested.
In this paper a detailed description of the new test facility for room-size humidity experiments is presented. The climatic chamber allows to perform both room buffer experiments for validation of coupled BES-HAM models, as well as experiments for the validation of CFD-HAM models. The generated data sets are available for other researchers. Additionally the detailed description may give insight in the design of future test facilities.
During the experiments, temperature and RH at different depths in a hygroscopic test sample installed in one of the walls of a room-size chamber, as well as the temperature and RH in the test room and of the supply air are measured. Preliminary experiments showed a good performance and repeatability of the experiments. Two types of experiments were run. In the first type of tests a jet enters the test room and blows onto the test sample. The supply air as well as the temperature outside the room is kept at a constant value of 25°C. The case can thus be considered as isothermal. Still the energy equation for the porous material needs to be solved simultaneously with the mass transport equation to capture the temperature change inside the material due to latent heat effect. A comparison between the measured temperature and RH inside the test sample and those computed with a recently developed CFD-HAM model, showed good agreement. Also measurements of the velocity field in the room were compared with simulation results. It was concluded that a quasi steady solution of the jet gives adequate

precision to solve the heat and moisture transport accurately. In the second type of experiments additional hygroscopic plates were introduced in the room while the temperature and RH in the middle of the test room was measured. Temperature of the supply air and outside the room was again kept constant. Again, a good agreement between the measured values and the results calculated with a recently coupled BES-HAM model was found.

6 Nomenclature

ACH	Air change rate (1/h)
C	Specific heat (J/kg·K)
D	Vapour diffusion coefficient in air (m²/s)
E	Energy (J/m³)
g	Vapour diffusion flux (kg/m²·s)
L	Latent heat of vaporization (J/kg)
p	Partial vapour pressure (Pa)
RH	Relative humidity (%)
R_v	Gas constant water vapour (J/kg·K)
T	Temperature (°C)
t	Time (s)
w	Moisture content (kg/m³)
Y	Mass fraction (kg/kg)

Greek symbols

λ	Thermal conductivity (W/m·K)
μ	Water vapour resistance factor (-)
ρ	Density (kg/m³)
ψ_0	Open porosity (%)

Subscripts

air	Air
liq	Liquid water
mat	Material
sat	Saturation
vap	Water vapour

7 Acknowledgement

The results presented in this paper have been obtained within the frame of the research project IWT-SB/51283/Steeman and IWT-SB/81322/VanBelleghem, and the IWT SBO-050451 project Heat, Air and Moisture Performance Engineering: A Whole Building Approach. All are funded by the Flemish Institute for the Promotion and Innovation by Science and Technology in Flanders. Its financial support is gratefully acknowledged.

8 References

[1] Fang L, Clausen G, Fanger PO. Impact of temperature and humidity on the perception of indoor air quality. Indoor Air-International Journal of Indoor Air Quality and Climate 1998;8:80-90.

[2] Simonson CJ, Salonvaara M, Ojanen T. The effects of structures on indoor humidity – possibility to improve comfort and perceived air quality. Indoor Air 2002;12:243-251.
[3] Pavlogeorgatos G. Environmental parameters in museums. Building and Environment 2003;38(12):1457-1462.
[4] Steeman HJ, Van Belleghem M, Janssens A, De Paepe M. Coupled simulation of heat and moisture transport in air and porous materials for the assessment of moisture related damage. Building and Environment 2009;44(10):2176-2184.
[5] Steeman M, De Paepe M, Janssens A. Impact of whole-building hygrothermal modelling on the assessment of indoor climate in a library building. Building and environment 2010;45:1641-1652.
[6] Osanyintola OF, Simonson CJ. Moisture buffering capacity of hygroscopic building materials: Experimental facilities and energy impact. Energy and Buildings 2006;38(10):1270-1282.
[7] Steeman M, Janssens A, De Paepe M. Performance evaluation of indirect evaporative cooling using whole-building hygrothermal simulations. Applied Thermal Engineering 2009;29(14-15): 2870-2875.
[8] Woloszyn M, Kalamees T, Olivier Abadie M, Steeman M, Sasic Kalagasidis A. The effect of combining a relative-humidity-sensitive ventilation system with the moisture-buffering capacity of materials on indoor climate and energy efficiency of buildings. Building and Environment 2009; 44(3): 515-524.
[9] Energy Conservation in Buildings and Community Systems (ECBCS). Annex 41 Whole Building Heat, Air and Moisture Response (MOIST-ENG). www.ecbcs.org/annexes/annex41.htm
[10] Woloszyn M, Rode C. IEA Annex 41: whole building heat, air, moisture response. Subtask 1: Modelling Principles and Common Exercises. Final report. ISBN: 978-90-334-7057-8; 2008.
[11] Hens H. IEA Annex 24: Heat, Air and Moisture Transfer in Insulated Building Envelopes. Task 1: Modelling. 1996.
[12] Steeman M, Hygrothermal modelling for building energy simulation applications. Ph.D. thesis, Ghent University, Belgium, 2010.
[13] Steeman M, Janssens A, Steeman HJ, Van Belleghem M, De Paepe M. On coupling 1D non-isothermal heat and mass transfer in porous materials with a multizone building energy simulation model. Building and Environment 2010;45:865-877.
[14] Steeman HJ. Modelling local hygrothermal interaction between airflow and porous materials for building applications. Ph.D. thesis, Ghent University, Belgium, 2009.
[15] Steeman HJ, Janssens A, Carmeliet J, De Paepe M. Modelling indoor air and hygrothermal wall interaction in building simulation: Comparison between CFD and a well-mixed zonal model. Building and Environment 2009;44(3):572-583.
[16] Steskens P. Modelling of the hygrothermal interactions in between the indoor environment and the building envelope. Ph.D. thesis, BYG-DTU Department of Civil Engineering, Technical University of Denmark, 2009.
[17] Mendonca K, Inard C, Wurtz E, Winkelmann FC, Allard F. A zonal model for predicting simultaneous heat and moisture transfer in buildings. 9th International Conference on Indoor Air Quality and Climate. Monterey, Canada, June 30-July 5, 2002.
[18] Hagentoft CE, Adl-Zarrabi B, Roels S, Carmeliet J, Hens H, Grunewald J, Funk M, Becker R, Shamir D, Adan O, Brocken H, Kumaran K, Djebbar R. Assessment method of numerical prediction models for combined heat, air and moisture transfer in building components. Journal of Building Physics 2004;27(4):327-352.
[19] Svennberg K, Hedegaard L, Rode C. Moisture buffer performance of a fully furnished room, ASHRAE Special Publications. Proceedings of Buildings IX Conference, 2004.
[20] Hedegaard L, Rode C, Peuhkuri R. Full scale tests of moisture buffer capacity of wall materials. 7th Nordic Building Physics Symposium, Reykjavic, Iceland, Vol.2, 662-669, 2005.

[21] Holm A, Kunzel HM. Experimental investigation of hygric buffering capacity of wood based interior panelling. Research in building physics and building engineering - Proceedings of the third international Building Physics Conference, Concordia University, Montreal, 2006.
[22] Yang X, Vera S, Rao J, Ge H, Fazio P. Full-scale experimental investigation of moisture buffering effect and indoor moisture distribution. Building X Conference, Florida, USA, 2007.
[23] Yoshino H, Mitamura T, Hasegawa K. Moisture buffering and effect of ventilation rate and volume rate of hygrothermal materials in a single room under steady state exterior conditions. Building and Environment 2009;44(7):1418-1425.
[24] Plathner P, Woloszyn M. Interzonal air and moisture transport in a test house: experiment and modelling. Building and Environment 2002;37(2):189-199.
[25] Oldengarm J. Field experiments on airborne moisture transport. Air Infiltration Review 1991;12(2):8-11.
[26] Simonson CJ. Moisture, thermal and ventilation performance of Tapanila ecological house. VTT Research notes 2069. Technical Research Centre of Finland. 2000.
[27] Hohota R. Moisture modelling CFD code (low velocity in large enclosure). Comparison with experiments (in French). Ph.D. thesis. Laboratoire CETHIL INSA de Lyon, France, 2003.
[28] Teodosiu C, Hohota R, Rusaou G, Woloszyn M. Numerical prediction of indoor air humidity and its effect on indoor environment. Building and environment 2003;38:655-664.
[29] Alturkistani A, Fazio P, Rao J, Mao Q. 2008. A new test method to determine the relative drying capacity of building envelope panels of various configurations. Building and Environment 2008;43(12):2203-2215.
[30] Sadauskiene J, Stankevicius V, Bliudzius R, Gailius A. The impact of the exterior painted thin-layer render's water vapour and liquid water permeability on the moisture state of the wall insulating system. Construction and Building Materials 2009;23(8):2788-2794.
[31] Fazio P, Athienitis AK, Marsh C, Rao J. Environmental Chamber for Investigation of Building Envelope Performance. Journal of Architectural Engineering 1997;3(2):97-102.
[32] Li Q, Rao J, Fazio P. Development of HAM tool for building envelope analysis. Building and environment 2009;44:1065-1073.
[33] Pavlik Z, Jirickova M, Cerny R. System for testing the hygrothermal performance of multi-layered building envelopes. Journal of Building Physics 2002;25:239-249.
[34] Pavlik Z, Cerny R. Hygrothermal performance study of an innovative interior thermal insulation system. Applied Thermal Engineering 2009;29:1941-1946.
[35] Dionisi Vici P, Mazzanti P, Uzielli L. Mechanical response of wooden boards subjected to humidity step variations: climatic chamber measurements and fitted mathematical models. Journal of Cultural Heritage 2006;7(1):37-48.
[36] Belarbi R, Qin M, Aït-Mokhtar A, Nilsson LO. Experimental and theoretical investigation of non-isothermal transfer in hygroscopic building materials. Building and Environment 2008;43: 2154-2162.
[37] Steeman HJ, Janssens A, De Paepe M. On the applicability of the heat and mass transfer analogy in indoor air flows. International Journal of Heat and Mass Transfer 2009;52(5-6):1431-1442.
[38] Talukdar P, Olutmayin SO, Osanyintola OF, Simonson CJ. An experimental data set for benchmarking 1-D, transient heat and moisture transfer models of hygroscopic building materials. Part I: Experimental facility and material property data. International Journal of Heat and Mass Transfer 2007;50(23-24):4527-4539.
[39] Talukdar P, Osanyintola OF, Olutimayin SO, Simonson CJ. An experimental data set for benchmarking 1-D, transient heat and moisture transfer models of hygroscopic building materials. Part II: Experimental, numerical and analytical data, International Journal of Heat and Mass Transfer 2007;50(25-26):4915-4926.

[40] Olutimayin SO, Simonson CJ. Measuring and modeling vapor boundary layer growth during transient diffusion heat and moisture transfer in cellulose insulation. International Journal of Heat and Mass Transfer 2005;48(16):3319-3330.
[41] Osanyintola OF, Talukdar P, Simonson CJ. Effect of initial conditions, boundary conditions and thickness on the moisture buffering capacity of spruce plywood. Energy and Buildings 2006;38(10):1283-1292.
[42] Iskra CR, Simonson CJ. Convective mass transfer coefficient for a hydrodynamically developed airflow in a short rectangular duct, International Journal of Heat and Mass Transfer 2007;50(11-12):2376-2393.
[43] Talukdar P, Iskra CR, Simonson CJ. Combined heat and mass transfer for laminar flow of moist air in a 3D rectangular duct: CFD simulation and validation with experimental data. International Journal of Heat and Mass Transfer 2008;51(11-12):3091-3102.
[44] Bednar T, Dreyer J. Determination of moisture surface transfer coefficients under transient conditions. Research in Building Physics - Proceedings of the second international conference on building physics, Antwerp, Belgium, 2003.
[45] ISOCAB. http://www.isocab.be
[46] Huang BJ, Liao YC, Kuo TC. Study of a new environmental chamber design. Applied Thermal Engineering 2007;27(11-12):1967-1977.
[47] Dooley JB, O'Neal DL. The transient response of capacitive thin-film polymer humidity sensors. HVAC & Research 2008;14:663-682
[48] Adam O, Brocken H, Carmeliet J, Hens H, Roels S, Hagentoft CE. Determination of liquid water transfer properties of porous building materials and development of numerical assessment methods. Introduction to the EC HAMSTAD project. Journal of Thermal Envelope and Building Science 2004;27:253-260.
[49] Roels S, Carmeliet J, Hens H. HAMSTAD WP1: Final report – Moisture transfer properties and materials characterization. Laboratory of Building Physics, KU Leuven. 2003.
[50] Steeman M, Van Belleghem M, De Paepe M, Janssens A. Experimental validation and sensitivity analysis of a coupled BES-HAM model. Building and Environment 2010;45(10):2201-2217.
[51] Steeman HJ, T'Joen C, Van Belleghem M, Janssens A, De Paepe M. Evaluation of the different definitions of the convective mass transfer coefficient for water evaporation into air. International Journal of Heat and Mass Transfer 2009;52(15-16):3757-3766.
[52] Van Belleghem M, Steeman HJ, Steeman M, Janssens A, De Paepe M. Sensitivity analysis of CFD coupled non-isothermal heat and moisture modelling. Building and Environment 2010;45(11):2485-2496.
[53] Zhai ZQ, Chen QY, Haves P, Klems JH. On approaches to couple energy simulation and computational fluid dynamics programs. Building and Environment 2002;37(8-9):857-864.

Figure 1. Schematic representation of the climatic chamber and the air handling unit (dimensions in cm): (1) recirculation fan, (2) cooling coil, (3) resistive heater, (4) steam humidifier, (5) buffer vessel and (6) flow straightener

Figure 2. View on the outer and inner test chamber with the test wall

Figure 3. Algorithm used to control the supply air temperature and relative humidity.

Figure 4. Response of the relative humidity sensor to a change of absolute humidity, at constant temperature (a) and response of the relative humidity sensor to a change of temperature, at a constant absolute humidity (b). Temperature indicated in green, relative humidity indicated in black.

Figure 5. Comparison between chilled mirror calibration (▲) and two-pressure calibration (■) for a capacitive sensor

Figure 6. Schematic representation of the calcium silicate test sample (a) and view on the test sample (b)

Figure 7. Influence of the cutting edge on the measured temperature and relative humidity in the sample: original sample (black line, with error bars) and adapted sample (green line). Measurements in the sample at 25mm (a,b), measurements at the front surface of the sample (c,d) and measurements at the back of the sample (e,f)

Figure 8. Comparison of the measured velocity in the middle of the room (a) and the simulated velocity (b). Velocities are indicated in m/s

Figure 9. Relative humidity (a) and temperature (b) at a depth of 10mm in the calcium silicate. Green line are the simulation results at 10mm, red dashed line is at 8.3mm, blue dashed line is at 11.5mm, black line with error bars corresponds with the measurements. Similar graphs for relative humidity (c) and temperature (d) at 25mm depth and relative humidity (e) and temperature (f) at 50mm depth. In (c,d) the green line corresponds with simulation results at 25mm, the red dashed line is at 23.2mm and the blue dashed line is at 26.6mm. In (e,f) the green line is again simulation results at 50mm, the red dashed line is at 47.7mm and the blue dashed line is at 52.5mm.

Figure 10. Layout of the calcium silicate plates in the test room: (a) view in the test room and (b) floor plan of the test room.

Figure 11. Measured (black) and simulated (green) relative humidity and temperature in the test room.

Table 1. Measured material properties of calcium silicate [44-45]

Table 1

Material property	Measured value
Density (kg/m³)	$\rho_{\mu\alpha\tau} = 270$
Thermal conductivity (W/mK)	$\lambda = 0.06 + 5.6\ 10^{-4} \cdot w$
Open porosity (-)	$\psi_0 = 0.894$
Water vapour resistance factor (-)	$\mu = [(0.33 + 2.49 \cdot 10^{-6} \cdot \exp(6.84 \cdot RH)]^{-1}$
Sorption isotherm (kg/m³)	$w = w_{sat}[1+(a\rho_{liq}R_vT\ln(RH))^n]^{(1-n)/n}$
Saturation moisture content (kg/m³)	$w_{sat} = 894$
	$a = -2.936*10^{-5}$
	$n = 1.7266$
Specific heat (J/kgK)	$C_{mat} = 1000$

Figure 1

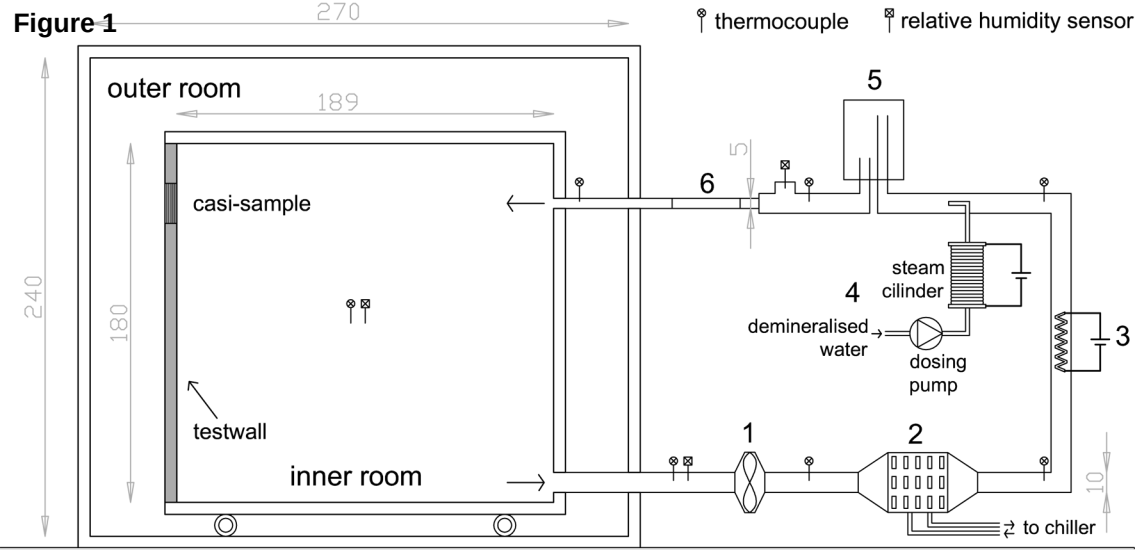
270
thermocouple
relative humidity sensor
outer room
189
240
180
casi-sample
testwall
inner room
5
6
5
steam
cilinder
4
demineralised
water
dosing
pump
3
1
2
10
to chiller

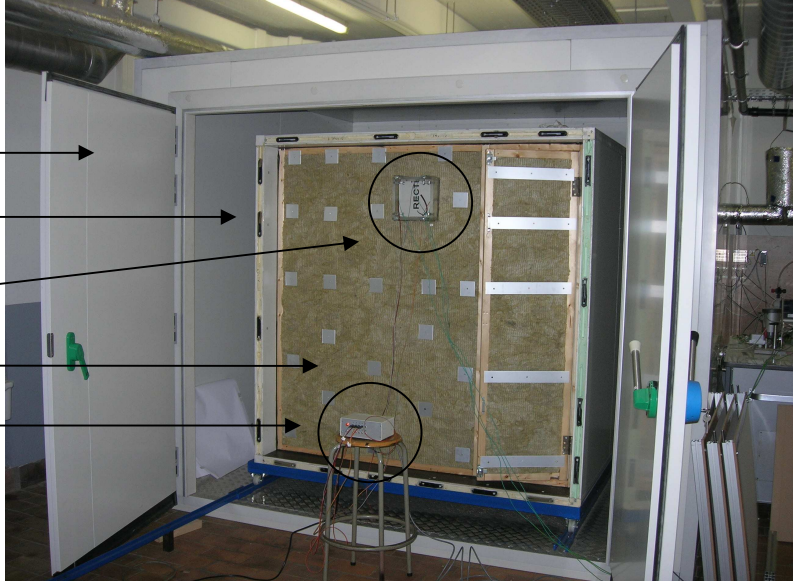
Outer room
Inner room
Test sample
Test wall
Data acquisition

Figure 3

Click here to download high resolution image

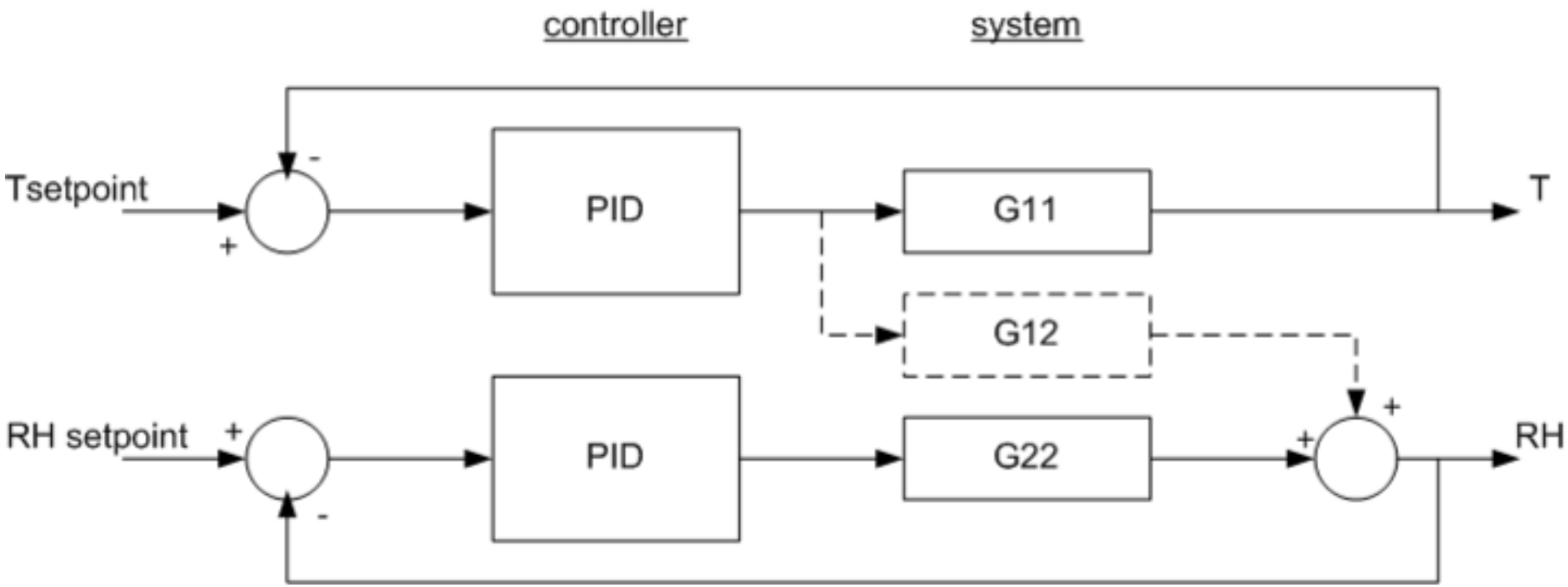

Figure 4a

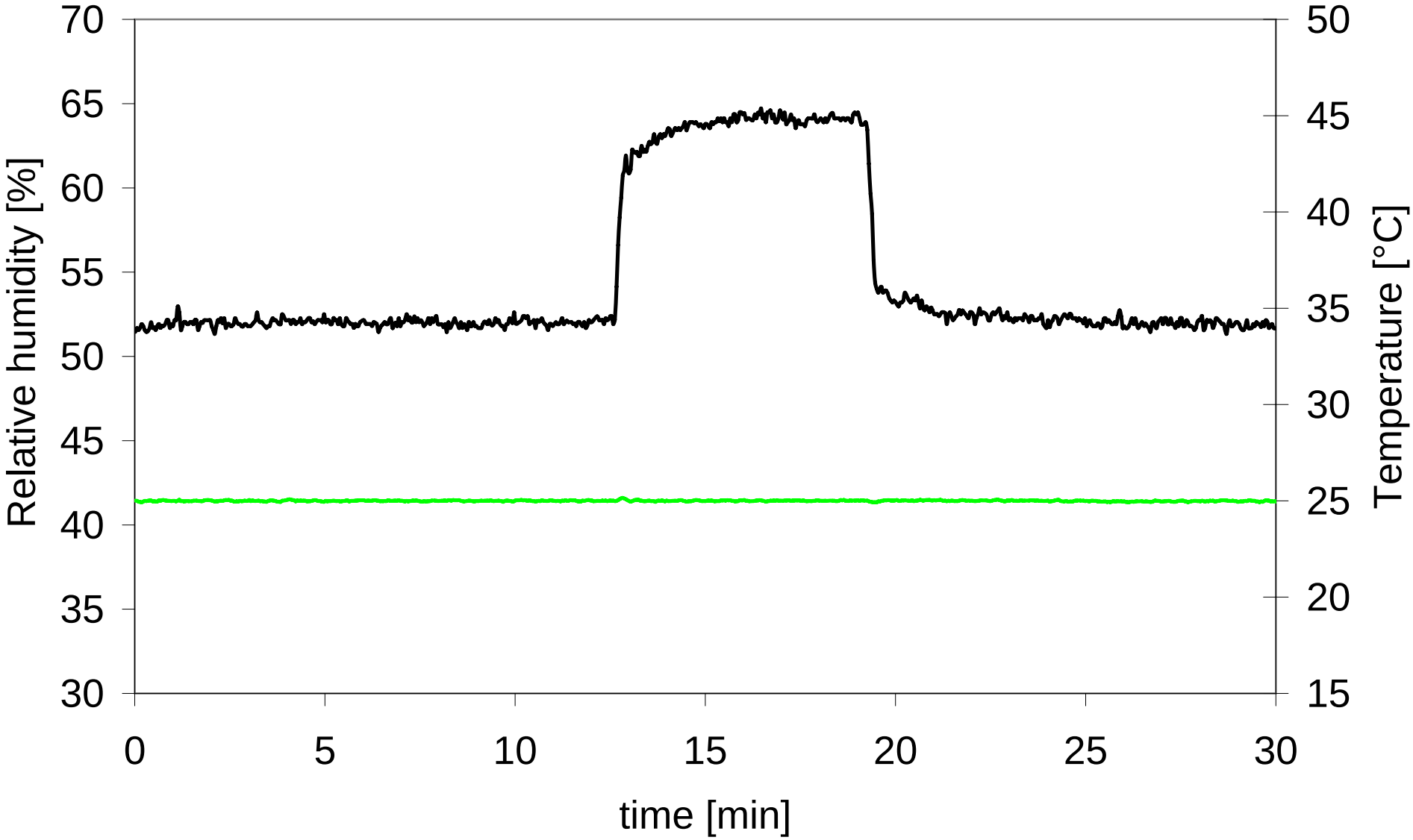
70
65
60
55
50
45
40
35
30
Relative humidity [%]
50
45
40
35
30
25
20
15
Temperature [°C]
0
5
10
15
20
25
30
time [min]

Figure 4b

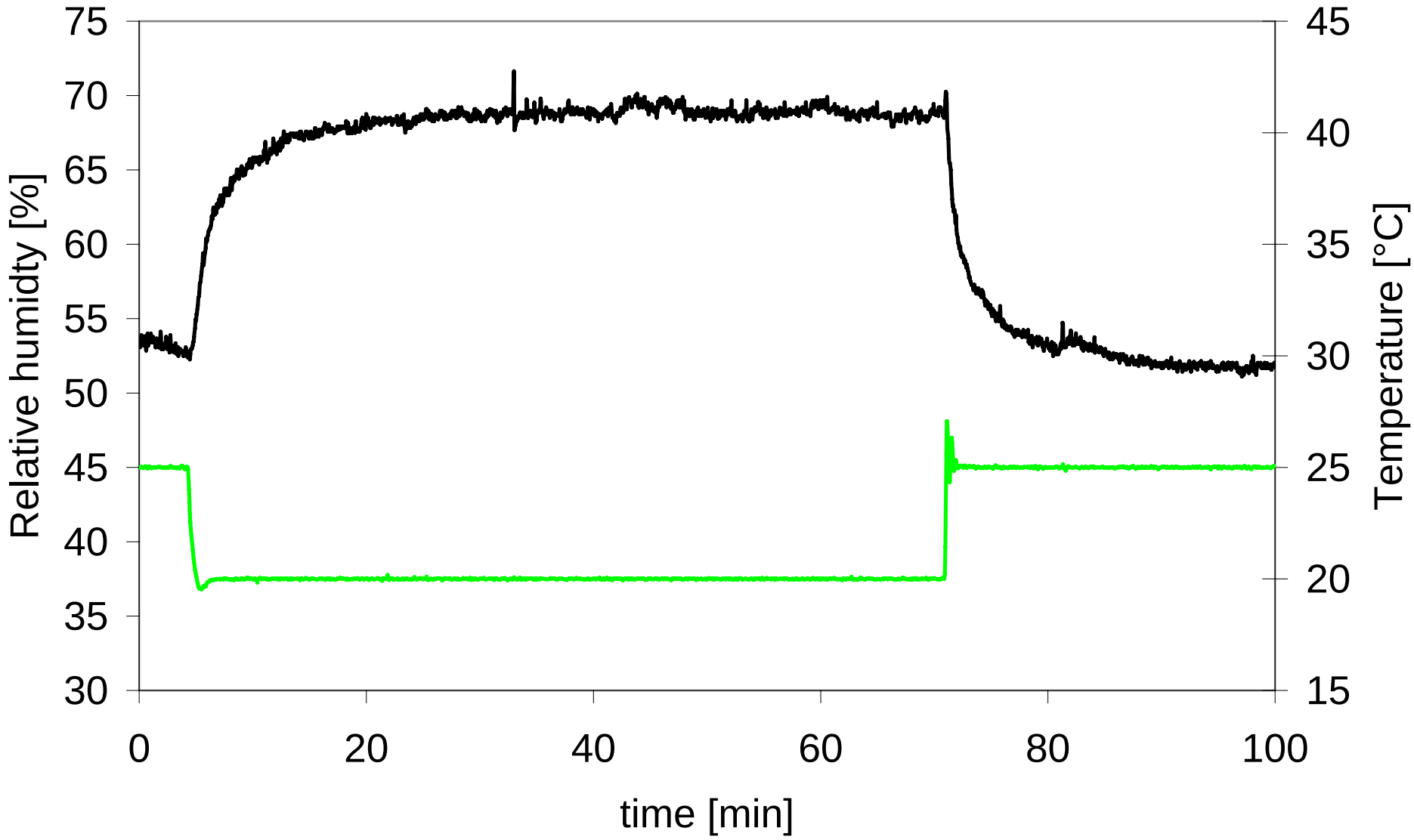
Relative humidty [%]
75
70
65
60
55
50
45
40
35
30
Temperature [°C]
45
40
35
30
25
20
15
0
20
40
60
80
100
time [min]

Figure 5

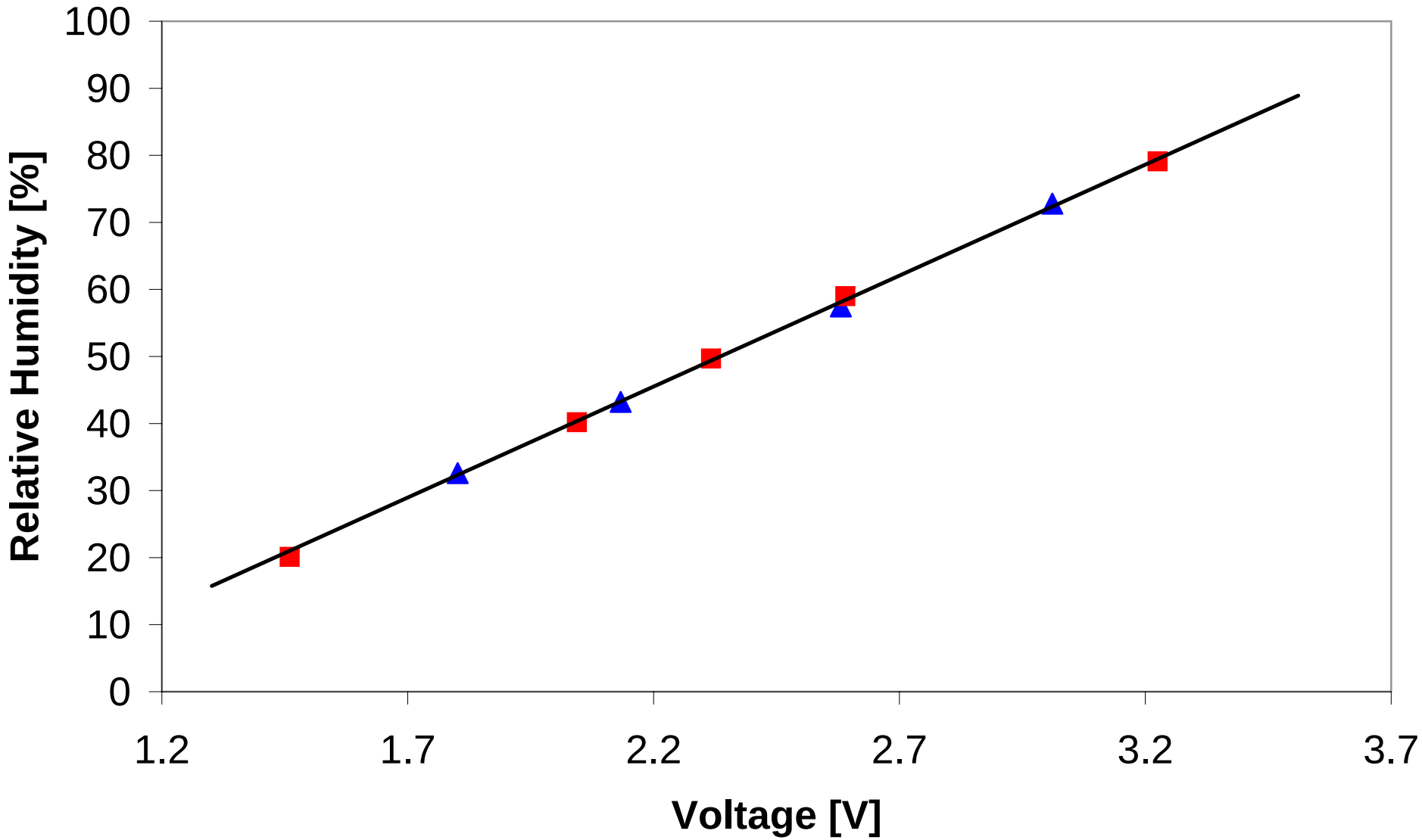
100
90
80
70
60
50
40
30
20
10
0
Relative Humidity [%]
1.2
1.7
2.2
2.7
3.2
3.7
Voltage [V]

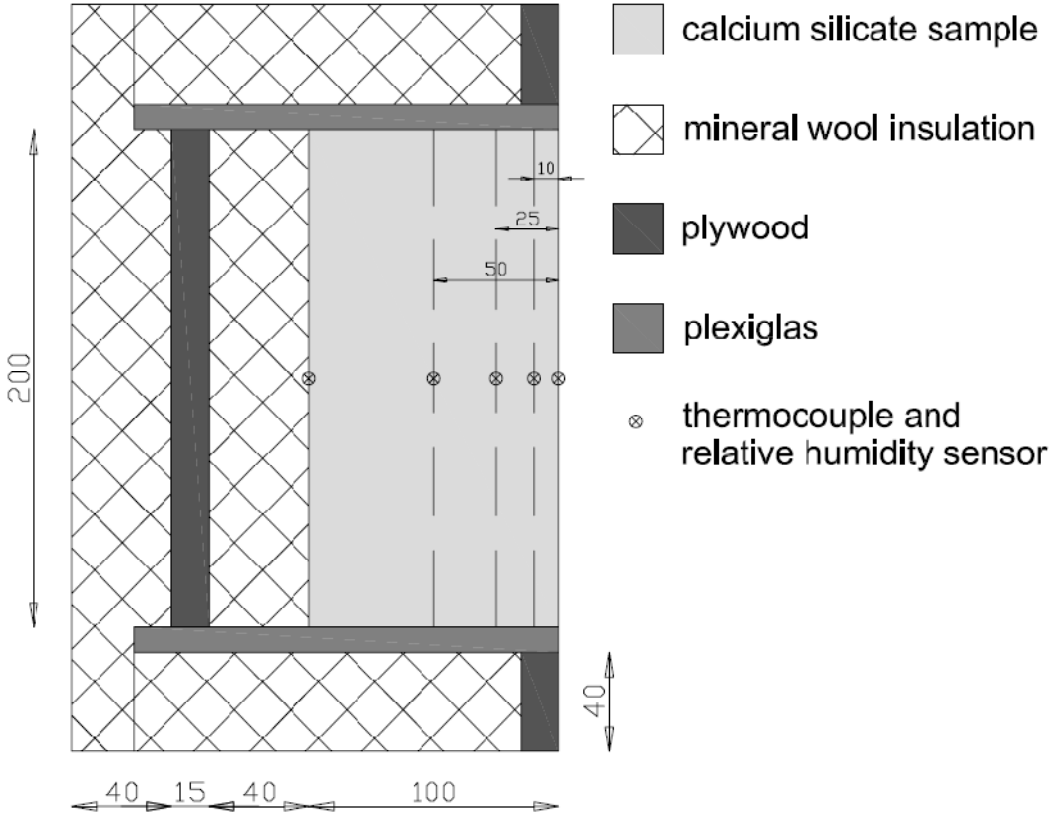
calcium silicate sample
mineral wool insulation
plywood
plexiglas
thermocouple and
relative humidity sensor
10
25
50
200
40
40
15
40
100

(a)

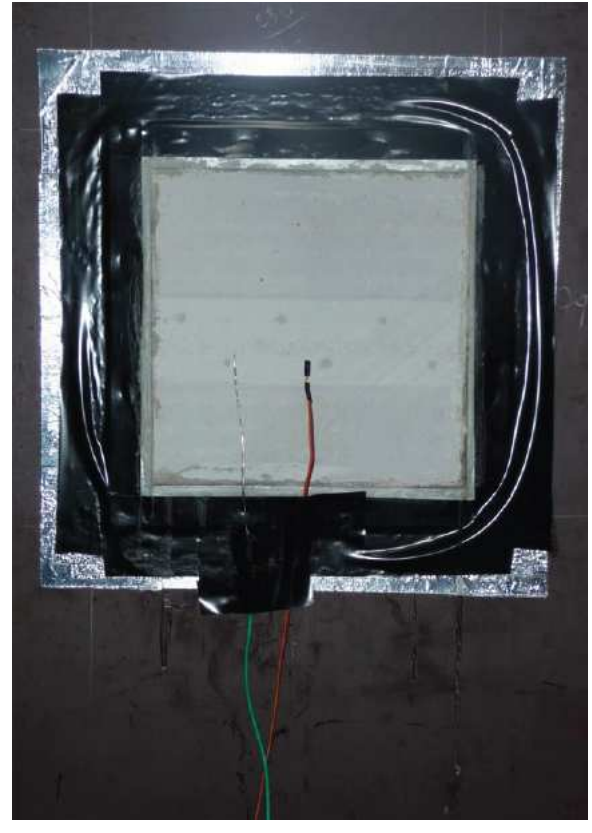

(b)

Figure 7

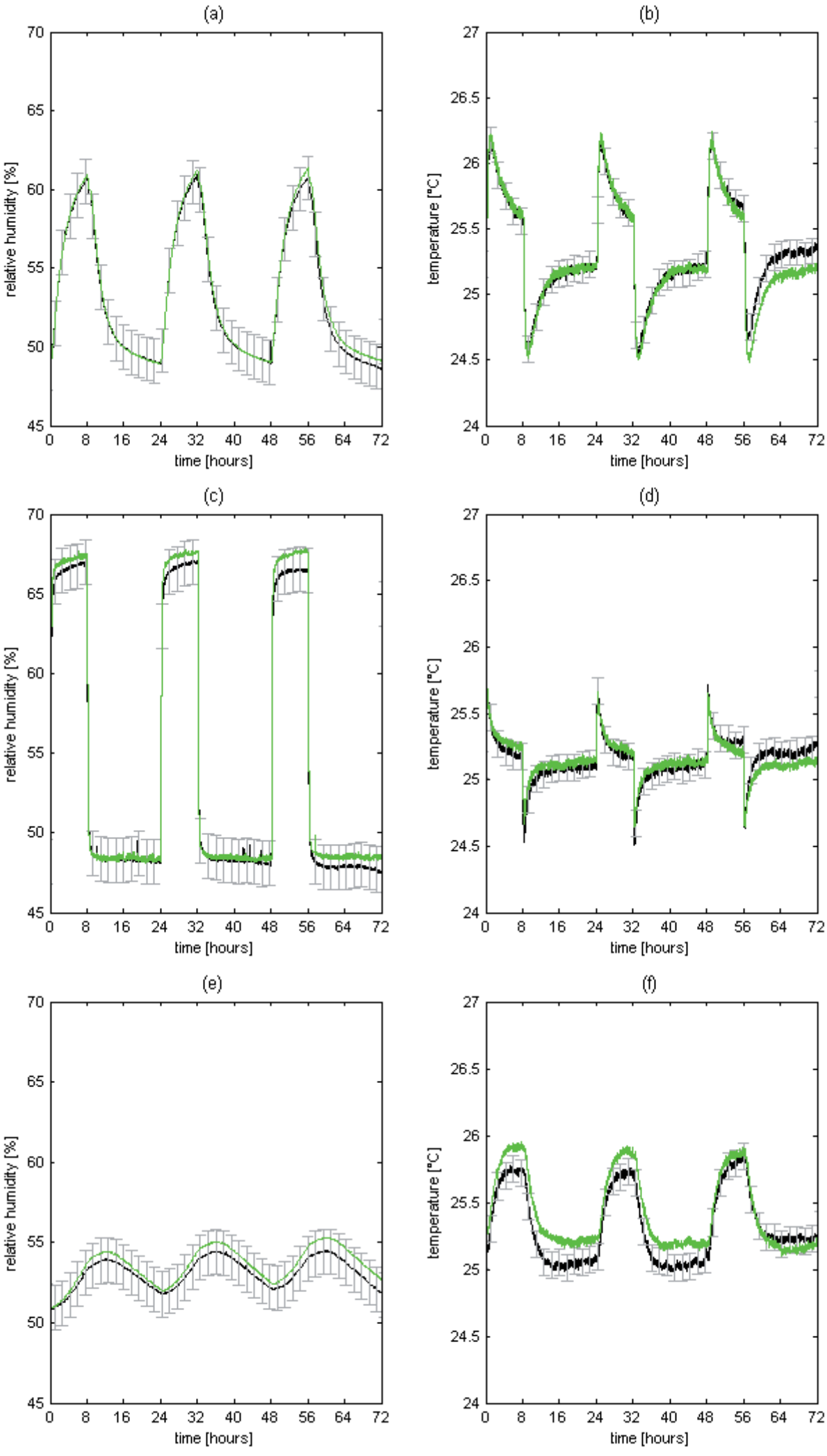
(a)
relative humidity [%]
time [hours]
(b)
temperature [°C]
time [hours]
(c)
relative humidity [%]
time [hours]
(d)
temperature [°C]
time [hours]
(e)
relative humidity [%]
time [hours]
(f)
temperature [°C]
time [hours]

Figure 8

Click here to download high resolution image

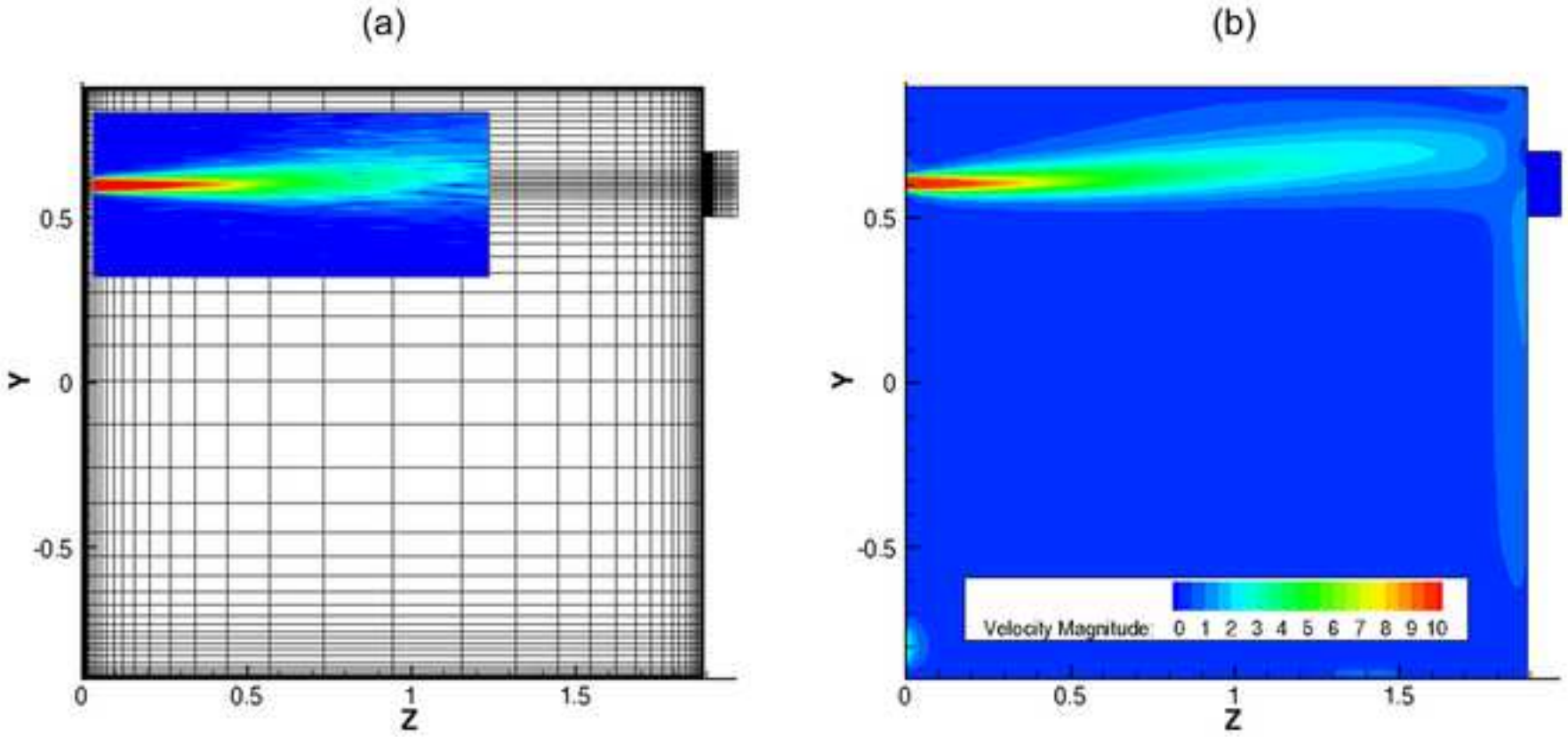

Figure 9

Click here to download high resolution image

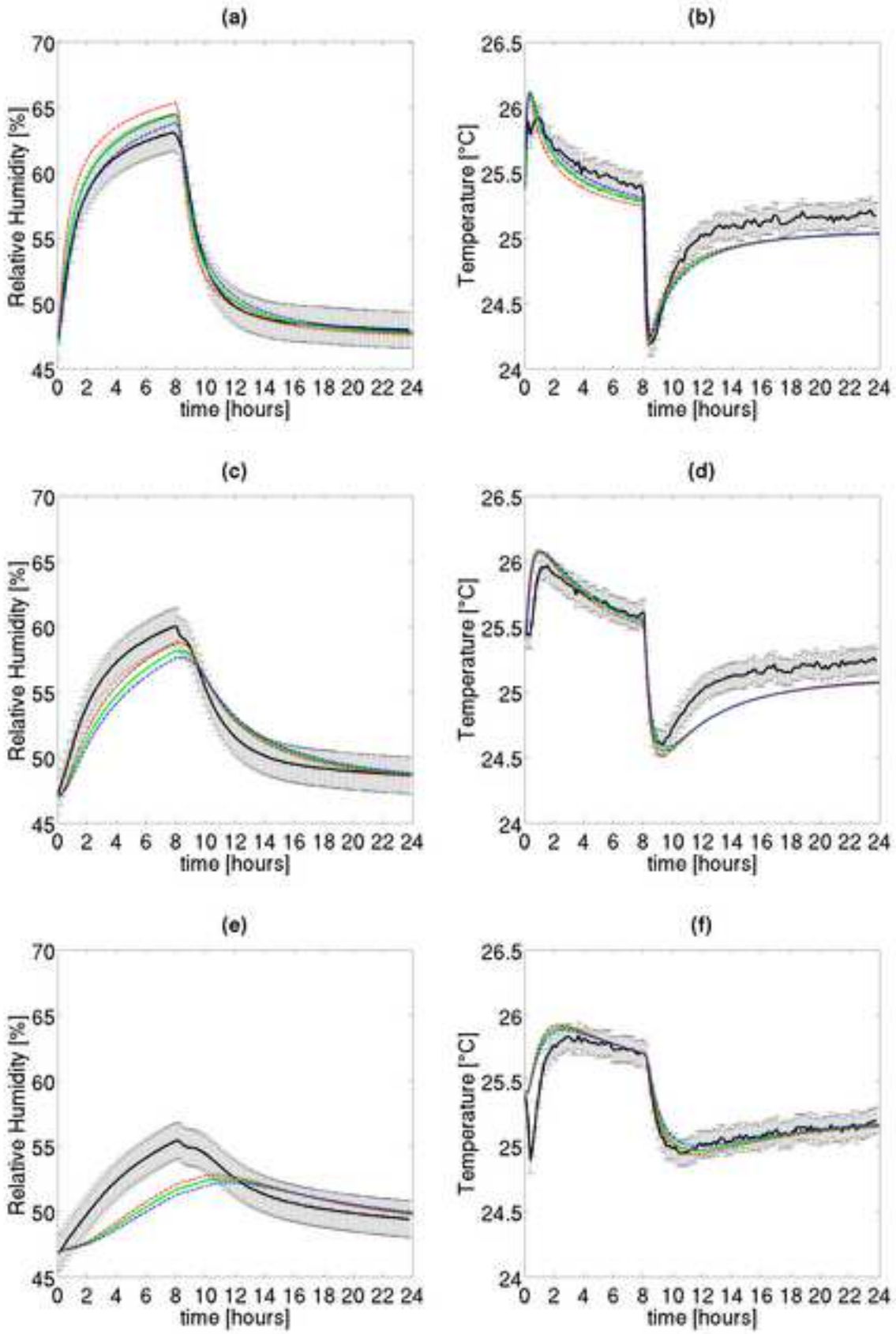

(a)

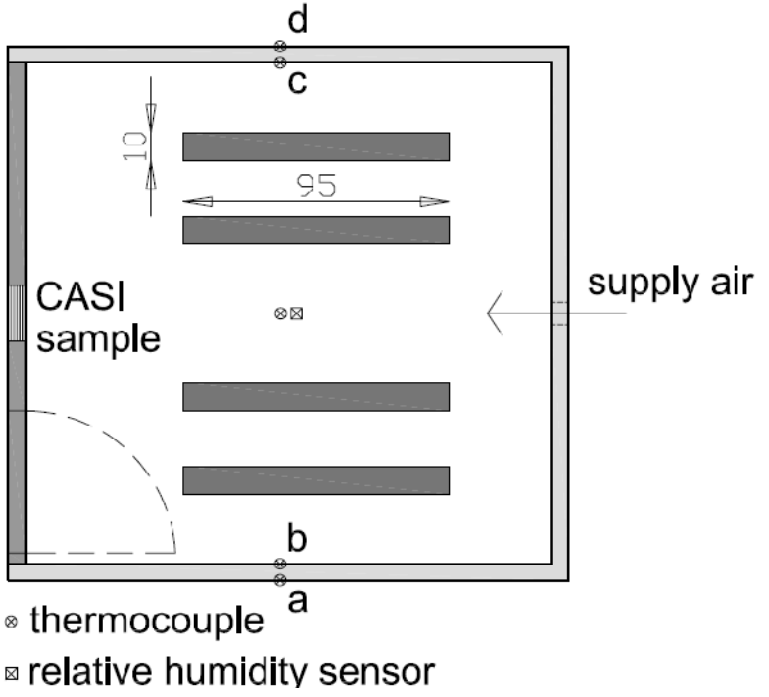
d
c
10
95
CASI
sample
supply air
b
a
thermocouple
relative humidity sensor

(b)

Figure 11

Click here to download high resolution image